

Structural Basis for the Enzyme-Polymer Binding Mechanism of Poly(vinyl alcohol) Esterase

Yanfei Wu,[¶] Xuexia Xu,[¶] Chao-Fan Yin,[¶] Zhuanglin Shen, Lanteng Wang, Ning-Yi Zhou,* and Jiahai Zhou*



Cite This: *ACS Catal.* 2025, 15, 11194–11203



Read Online

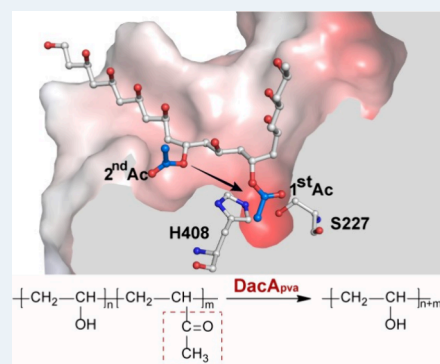
ACCESS |

Metrics & More

Article Recommendations

Supporting Information

ABSTRACT: Structural characterization of microbial enzymes involved in plastic transformation and modification is of significant importance, yet has been hindered by the challenges in obtaining enzyme-plastic complex structures. Poly(vinyl alcohol) (PVA), a typical C–C backbone hydrophilic polymer, offers a potential for obtaining enzyme-polymer complexes. DacA_{pva}, a unique PVA deacetylase, was recently identified from PVA utilizer *Comamonas* sp. strain NyZ500. However, the molecular basis of PVA binding and deacetylation by DacA_{pva} remains unknown. Here, we determined high-resolution crystal structures of DacA_{pva} and its complex with acetylated PVA. A distinctive hydrophobic platform and enhanced serine interactions were found to be crucial for stable substrate binding in the active site, which differed from the previously reported arginine interactions in this class of enzymes. A plausible model of DacA_{pva} was proposed for serine prebinding and the sequential removal of acetyl groups by sliding PVA C–C backbone based on biochemical and computational approaches. Our study presents a valuable framework for investigating the enzymatic deacetylation of C–C backbone polymers and has promising implications for the development of efficient plastic-modifying enzymes.



KEYWORDS: poly(vinyl alcohol), plastic modification, complex structure, biocatalysis, enzyme-polymer binding, molecular mechanism

INTRODUCTION

The global ecosystem is facing a significant threat from plastic pollution, as evidenced by numerous studies.¹ To address this issue, a number of scientists have suggested the use of biochemical catalysis as a viable solution to plastic recycling and upcycling.^{2–5} Poly(vinyl alcohol) (PVA) is a biodegradable but fossil-based polymer commonly known as “bioplastic”.⁶ Commercial PVA with varying content of acetyl groups has a wide range of applications, including wood processing, construction, paper adhesives, architectural coatings, and pharmaceutical biomaterials.^{7,8} Synthesis of PVA polymer involves the polymerization of vinyl acetate with free-radical initiators and the removal of acetylated side chains.⁹ However, the conventional industrial deacetylation process involves saponification under strong basic and organic conditions, leading to severe pollution⁹ (Figure S1). Enzymatic reactions are widely acknowledged as an alternative, eco-friendly approach to chemical reactions in polymer transformation and modification.^{10,11} However, lack of these industrially-important enzymes has impeded their applications and associated engineering.^{12,13} PVA derivatives are commonly considered biodegradable, and the enzymatic cleavage of their backbone has been extensively studied.^{14,15} However, the acetyl content directly impacts the hydrophobic properties of PVA derivatives, which in turn significantly affects their biodegradability.⁹ The efficient deacetylation of PVA had

remained poorly understood until a highly active PVA deacetylase, DacA_{pva}, was recently discovered in PVA utilizer *Comamonas* sp. strain NyZ500.¹⁶ This deacetylase holds a high potential for the biotechnological modification of PVA and its derivatives. It opens up possibilities for the use of DacA_{pva} in the development of PVA-based materials with tailored properties for various commercial applications. This enzyme contains a functionally unassigned N-terminal domain and a C-terminal domain, being classified within the GDSL-like Lipase/acylhydrolase 2 family (PF13472).¹⁷ The majority in this family (as many as 157,617 entries (May 2025)) function as xylan/cellulose deacetylase,¹⁸ whereas DacA_{pva} is the only one so far proven to primarily recognize C–C backbone polymer substrate rather than oligosaccharides. In this family, resolved enzyme complex structures are particularly rare, with only three reported oligosaccharide complex structures of esterases CtCE2 with cellobiose,¹⁹ PbeAxCE with MeGlcA-Xylp,²⁰ and RiCE17 with mannopentaose.²¹

Received: March 10, 2025

Revised: June 4, 2025

Accepted: June 5, 2025

Understanding of the plastic-modifying mechanism has long been of interest but is challenging due to the difficulty of obtaining enzyme-polymer complex structures. The good solubility of PVA in this study makes it have high potential for us to obtain enzyme-polymer complexes. In this study, we present crystal structures of DacA_{pva} in apo form and complexes of DacA_{pva} with PVA at different lengths of carbon chain, as well as with an intermediate and product acetate from PVA degradation, providing a detailed understanding of the molecular interactions between DacA_{pva} and PVA polymer as well as its derivatives. These structures of DacA_{pva} elucidate the way the enzyme binds to the C–C backbone polymer and the molecular model for acetylated polymer PVA deacetylation, providing a structural model for enzyme engineering in plastic modification.

EXPERIMENTAL METHODS

Chemicals and Genetic Manipulation. The supplies of substrates are given in Table S1. Oligonucleotide primers were purchased from Tsingke Bio Co., Ltd. (Beijing, China) and are listed in Table S2. The enzymes used for DNA manipulation, including DNA polymerase and restriction enzymes, were purchased from Vazyme Biotech Co., Ltd. (Nanjing, China). The crystallization kits were purchased from Hampton Research (USA).

Protein Expression and Purification. The sequence-validated constructs were transformed into *E. coli* BL21(DE3) by a standard procedure. The recombinant strain was cultured in Lysogeny broth (LB) with kanamycin (50 $\mu\text{g}\cdot\text{mL}^{-1}$) at 180 rpm and 37 °C until an OD₆₀₀ of 0.8 was reached and then induced with 0.1 mM isopropyl- β -D-thiogalactopyranoside (IPTG) for further incubation at 16 °C overnight. After the cells were collected by centrifugation, the harvested cells were resuspended in a buffer of 50 mM Tris-HCl (pH 8.0) containing 400 mM NaCl, 20 mM imidazole, and 10% glycerol and lysed by high-pressure homogeneous lysis (Union-Biotech Co., Ltd., Shanghai, China). Protein purification was conducted using a nickel-affinity column. The recombinant protein was eluted with 50 mM Tris-HCl (pH 8.0) and 400 mM NaCl, 250 mM imidazole, and 10% glycerol. The purification was verified by SDS-PAGE, and the protein concentration was measured by a NanoDrop One (Thermo Scientific, USA). Except for the DacA_{pva} variant with N-terminal domain truncation, which fails to be expressed, all other mutations can be expressed and purified (Figure S2). The protein used for crystallization was further purified through size exclusion chromatography (Superdex 200 Increase 10/300 GL), and then concentrated to 15–20 $\text{mg}\cdot\text{mL}^{-1}$ in 50 mM Tris-HCl (pH 8.0), 400 mM NaCl, and 5% glycerol (Figure S3A).

Crystallization and Structure Determination of DacA_{pva}. DacA_{pva} protein was crystallized by the sitting drop vapor diffusion technique at 16 °C. Initially, a stretch of 45 amino acids in the N-terminal of DacA_{pva} was truncated based on the analysis of predicted structures to assist protein crystallization (Figure S3D). Protein crystals of truncated DacA_{pva} were successfully obtained (Figure S3B) after incubation under the conditions listed in Table S3. Diffraction data were collected at the BL19U1 beamline at Shanghai Synchrotron Radiation Facility (Shanghai, China) (Figure S3C). The data were processed with HKL3000²² and XDS.²³ The DacA_{pva} crystal diffracted to 1.8 Å resolution and belonged to the space group *I*23, with unit-cell parameters of $a = 164.0$

Å, $b = 164.0$ Å, $c = 164.0$ Å, and $\alpha = \beta = \gamma = 90.0^\circ$. The structure was phased by PHASER²⁴ using predicted DacA_{pva} coordinates by the AlphaFold 3 server as the searching model. Then, the manual model building was carried out using COOT.²⁵ The model was refined by the program PHENIX-refine.²⁶ After multiple rounds of refinement, the crystallographic statistics results were generated by Phenix.table one,²⁷ as shown in Table S4. Graphical illustrations were created with PyMOL. Electrostatic surface potentials were calculated by the PyMOL Adaptive Poisson–Boltzmann Solver (APBS) electrostatics plugin (Version 3.0, Schrödinger, LLC). The crystal structure of the DacA_{pva} protein was similar to the predicted protein structure (Figure S3D).

Structure Determination of DacA_{pva} in Complex with PVA1788. PVA1788 (Degree of alcoholysis: 88%, degree of polymerization:1700) particles were dissolved in 50 mM Tris-HCl (pH 8.0), 400 mM NaCl, and 5% glycerol at concentrations of 3.5% (w/v) and 9% (w/v), consistent with the protein solution buffer composition (Table S3). Small molecular substrates, including D-sorbitol hexaacetate and β -D-maltose octaacetate, were also dissolved in the same buffer at 10–20 molar fold excess relative to the protein concentration. Then these substrates were incubated with protein solution containing purified DacA_{pva} for 1 h, followed by centrifugation at 12,000 \times g for 5 min at 4 °C to remove precipitates. Complexes with the aforementioned substrates were attempted to be obtained by conventional cocrystallization or crystal soaking methods. However, only the complex with hydrophilic polymer PVA1788 was obtained via cocrystallization by the sitting drop vapor diffusion technique at 16 °C. The data collection and refinement process were the same as aforementioned for the apo form structure.

Site-Directed Mutagenesis. Designated mutations were introduced by PCR amplification using the specific primers listed in Table S2 and pET28-DacA_{pva} as a template. The PCR products with the mutation were incubated with *DpnI* (New England Biolabs Inc., USA) to remove the template. The purified PCR products with mutations were introduced into *E. coli* DH5 α to form a circular plasmid. The mutations were verified by DNA sequencing.

Enzymatic Activity Assay. The enzymatic reaction was conducted at 37 °C for 5 min in the reaction mixture (500 μL) comprising 50 mM Tris-HCl (pH 8.0), 3% (w/v) polymer substrates or 5 mM small molecular substrates, and appropriate enzyme concentration. The reaction was then terminated by adding an equal volume of acetonitrile and subjected to HPLC analysis. The HPLC (Waters, USA) equipped with an organic acid analysis column (Aminex HPX-87H, 300 mm \times 7.8 mm, 9 μm ; Bio-Rad, USA) was used to analyze the acetate produced from substrates deacetylation. The single mobile phase of 5 mM H₂SO₄ was used to elute products with a flow rate of 0.6 $\text{mL}\cdot\text{min}^{-1}$ at 50 °C. The detection wavelength was 210 nm. Under these conditions, the retention time of acetate was 14.80 min. One unit of activity was defined as the amount of enzyme required to produce 1 μmol of acetate per minute at 37 °C. All enzymatic experiments were carried out at least in triplicate.

Molecular Docking. The DacA_{pva} protein structure was initially predicted using the AlphaFold 3 server.²⁸ Both the protein and ligand structures were converted into the PDBQT format (required for docking) using AutoDockTools v1.5.6.²⁹ The protein was processed by adding hydrogen and charges, and the ligands were prepared by adding atomic charges and

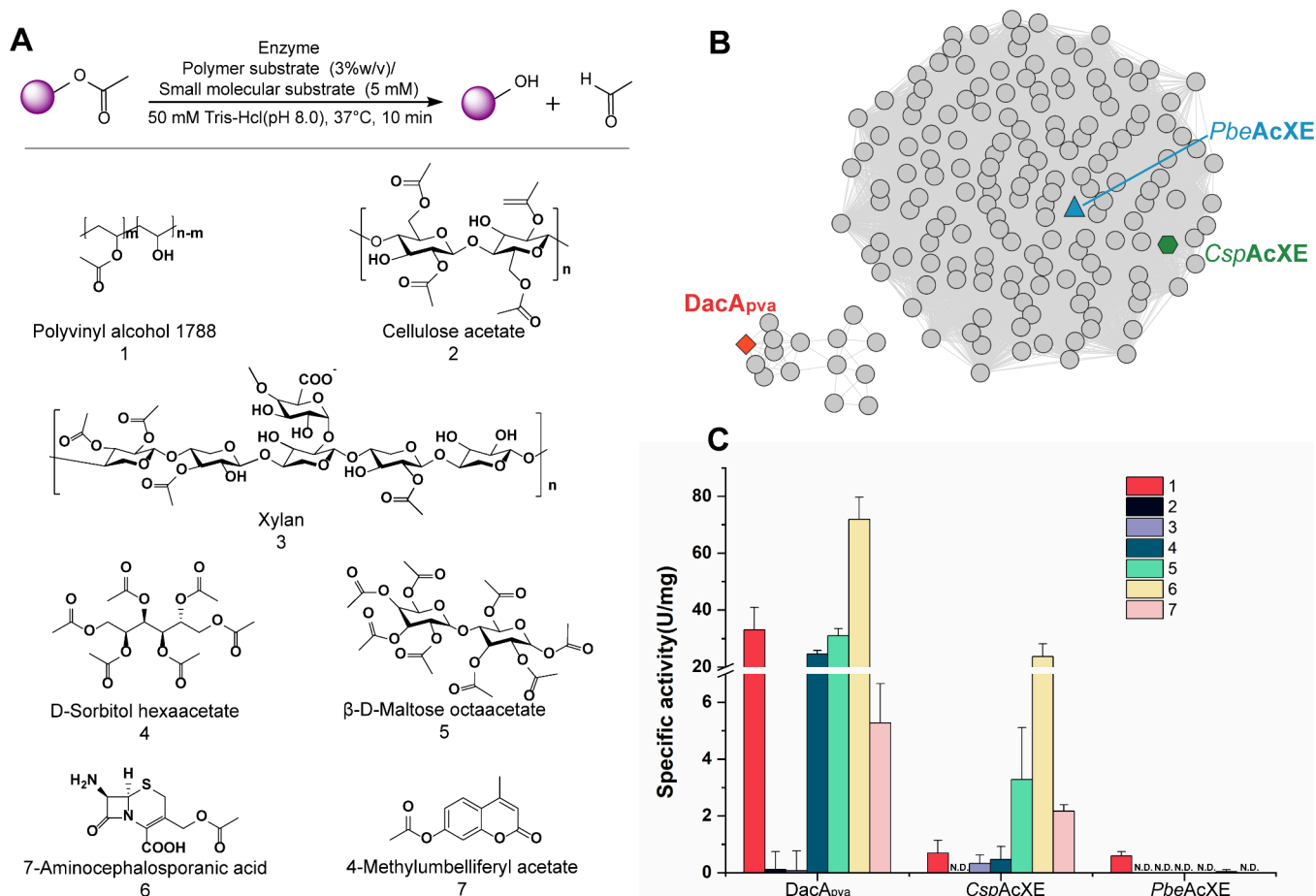


Figure 1. Substrate scope and activity assay of DacA_{pva} together with its homologous enzymes. (A) In vitro enzyme-catalyzed deacetylation of O-acetylated polymers and small molecules. (B) Sequence similarity network of DacA_{pva} and its homologous enzymes, including CspAcXE and PbeAcXE. (C) Deacetylation activity assay with different substrates, and the activities are given as the standard deviation of three replicates.

assigning atom types. The docking pocket was determined using AutoGrid,²⁹ and molecular docking was carried out using AutoDock Vina^{29,30} to search for the best docked conformation.

Binding Free Energy Calculation. The binding free energy of C22-DacA_{pva} and C22 mutants was calculated through an automated workflow termed Uni-GBSA,³¹ which employs the MM/GBSA (Molecular Mechanics/Generalized Born Surface Area) method with default parameters. This approach estimates the binding affinity by calculating the free energy difference (ΔG) among the protein–ligand complex, the isolated protein, and the ligand. The formula used is $\Delta G = \Delta G(\text{complex}) - \Delta G(\text{protein}) - \Delta G(\text{ligand})$.

Targeted Molecular Dynamics (TMD) Simulations. The molecular docking was performed to build the initial and targeted complex structures for further computational calculations. These two active MD coordinates obtained above served as the initial structure and the target one, respectively. Targeted molecular dynamics (TMD)³² was then carried out in the NPT ensemble implemented in the NAMD 2.14 package.³³ Moreover, the NPT ensemble was utilized at a constant temperature of 300 K and a constant pressure of 1 bar. Nonbonding interactions were handled with a 12 Å atom-based cutoff. The Particle Mesh Ewald (PME) method³⁴ was applied to treat electrostatic interactions with a 12 Å nonbonded cutoff. The force constants (10 kcal·mol⁻¹·Å⁻²) and 1 ns simulation time were tested to determine the optimal

TMD conditions. The integration step for the TMD simulations was set to 2 fs. For analysis, the trajectories were saved at intervals of 1 ps. Simulations were started from the inactive crystal structure to the active crystal structure. The TMD simulation was carried out with force constants of 10 kcal·mol⁻¹·Å⁻², in which the simulation times were 1 ns. Then, we performed a 200 ns conventional MD simulation based on the TMD structure to ensure the stability of the TMD structure. The binding free energy is calculated by the MM/GBSA³⁵ module in AmberTools22.³⁶

RESULTS AND DISCUSSION

Substrate Recognition of DacA_{pva} and Its Homologous Enzymes. As previously reported, DacA_{pva} was capable of hydrolyzing acetylated polymers, including polyvinyl acetate, poly(vinyl alcohol) 1788 (PVA1788) (1), and acetyl xylan (3), as well as small molecule 7-aminocephalosporanic acid (6).¹⁶ When testing its substrate scope in this study, DacA_{pva} was found to deacetylate a variety of other O-acetylated polymers and small molecules, including cellulose acetate (2), sorbitol hexaacetate (4), maltose octaacetate (5), and 4-methylumbelliferyl acetate (7) (Figure 1A). As a specific de-O-acetylase, DacA_{pva} was not active against N-acetylated and S-acetylated compounds as well as ester-bond containing compounds, polyethylene terephthalate (PET) and PET hydrolysates (Figure S4).

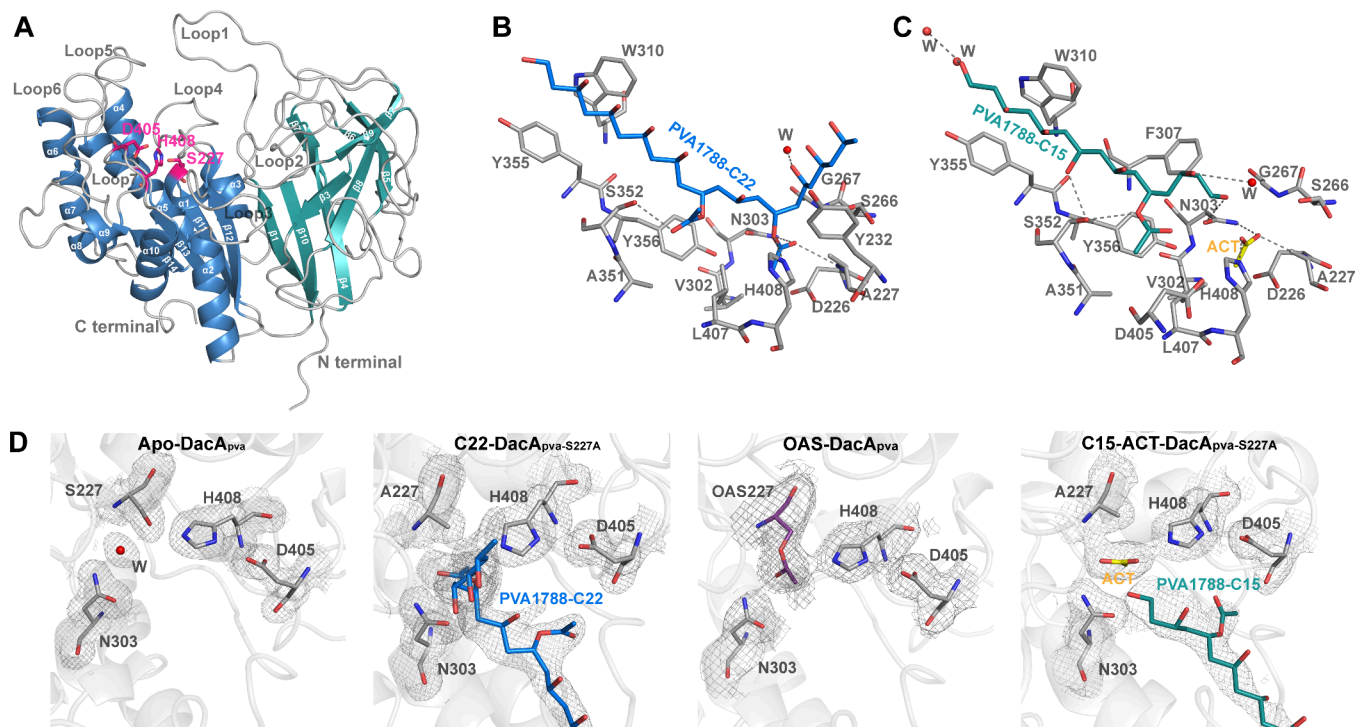


Figure 2. Structure of DacA_{pva} . (A) Overall structure of the apo-form DacA_{pva} . The C-terminal domain and N-terminal domain are displayed in blue and green, respectively. The loops are displayed in gray. The catalytic triad is shown as purple sticks. (B, C) Substrate-binding pockets of the crystal structure of $\text{DacA}_{\text{pva-S227A}}$ in complex with the substrate of PVA1788-C22 (blue in B), PVA1788-C15 (green in C) and the product of acetic acid (ACT) (yellow in C). The residues around the ligands are shown as gray sticks. (D) Omit map $2mF_o - DF_c$ for active sites and ligands in the crystal structures. The maps are shown as gray mesh (1σ).

Meanwhile, DacA_{pva} homologues were retrieved from the PDB database to investigate the substrate specificity of the other members of the GDSL-like Lipase/acylhydrolase 2 family. Among them, *PbeAcXE* from *Prolixibacter bellariivorans* and *CspAcXE* from *Chryseobacterium* sp. YR480,²⁰ sharing respective 33 and 39% sequence identity with DacA_{pva} , has been shown to function in the de-*O*-acetylation of per-acetylated xylooligosaccharide. While *PbeAcXE* and *CspAcXE* are clustered together in the sequence similarity network, DacA_{pva} is separated from the above two enzymes to form a significantly smaller category with limited homology (Figure 1B). Functionally, DacA_{pva} was indeed different from the majority of de-*O*-acetylating enzymes in the GDSL-like Lipase/acylhydrolase 2 family, primarily targeting C–C backbone polymers rather than glycan ones.²⁰ To further analyze the substrate recognition of DacA_{pva} and its homologous enzymes, the enzyme activities toward a variety of polymers and small molecules were investigated by an in vitro analysis. As illustrated in Figure 1C, both DacA_{pva} and *CspAcXE* were capable of hydrolyzing the *O*-acetyl side chain of different substrates, suggesting that these two esterases exhibit similar activity profiles regardless of substrate size. Whereas *PbeAcXE* was found to have activity toward PVA1788 only. Notably, the enzyme activity of DacA_{pva} was found to be significantly higher than that of *CspAcXE* and *PbeAcXE* on various substrates, especially with almost 50 times higher activity toward its native substrate PVA1788. Furthermore, DacA_{pva} displayed a preference for C–C backbone polymer substrates over xylan substrates. These differences in substrate recognition are likely due to variations in binding amino acids around enzyme pockets, similar to most cases reported.³⁷ This distinctive difference between DacA_{pva} and other GDSL-like Lipase/

acylhydrolase 2 family members led us to seek comprehensive structural insights into DacA_{pva} for unraveling its inherent functional attributes and unique characteristics.

Subsequently, molecular docking was applied to characterize interactions between AlphaFold 3-predicted DacA_{pva} and PVA1788. It turned out that the resulting top-ranked poses positioned substrate molecules distally from the canonical catalytic triad (S227-D405-H408) (Figure S5), suggesting a limited performance for computational methods in predicting or identifying open and extant substrate-binding pockets in this case.

Overall Structure of DacA_{pva} . To obtain crystals of DacA_{pva} , recombinant protein was heterologously expressed in *Escherichia coli* BL21(DE3), and purified using a combination of affinity and size exclusion chromatography (Figure S3A–C). Size exclusion chromatography analysis confirmed the monomer status of DacA_{pva} (Figure S3A). Guided by secondary structure and 3D structure prediction information (Figure S3D), we opted to truncate 45 amino acids from the N-terminus of DacA_{pva} to enhance protein crystallization. The enzyme assay verified no activity difference between the full-length DacA_{pva} and its truncated version (Table S5). In subsequent studies, this truncated DacA_{pva} is termed the wide type (WT). Subsequently, the DacA_{pva} was successfully crystallized and diffraction data were collected at a resolution of 1.8 Å (Table S4). Due to the low sequence similarity to previously resolved protein structures, the 3D structure prediction by the AlphaFold 3 server²⁸ was used for phasing. In the crystal structure of DacA_{pva} , its N-terminal domain contains a ten-stranded β -sheet ($\beta 1$ – $\beta 10$), while its C-terminal domain with a four-stranded β -sheet sandwiched between two layers of α -helices (Figure 2A). A prominent, huge groove

extends across the surface between the two domains to form an open binding pocket. The loops of the protein around the periphery of the groove resemble the lace of a bowl (Figure 2A), formed with loop1 (residues 52–72) from β 1 leading into β 2, loop2 (residues 164–180), loop3 (residues 231–241), loop4 (residues 265–282), loop5 (residues 308–318), loop6 (residues 344–358), and loop7 (residues 402–410).

Similar to the SGNH superfamily hydrolases, DacA_{pva} contains the conserved SGNH motif and GDSI motif in the C-terminal domain. Additionally, the classical catalytic triad (S227-D405-H408) of DacA_{pva} is in the C-terminal domain near the huge groove surface, with D405 and H408 in loop 7, and S227 in the α 1. In contrast, the fold of the N-terminal domain was found to be varied in most SGNH/GDSL hydrolases by multiple sequence alignment analysis (Figure S6). This phenomenon was also found at the structural level, where the SGNH hydrolase fold was commonly present in the catalytic domain of acetylxylan esterases from the carbohydrate esterase (CE) family of the SGNH superfamily (Figure S7). Nevertheless, the N-terminal domain (residues 45–219) of DacA_{pva} exhibits a unique jelly roll β -sandwich fold that does not resemble most known domains (Figure S7). This structural β -sandwich fold is intimately linked to the catalytic domain, forming a bowl-shaped open pocket.

Most DacA_{pva} homologous proteins exhibit significant structural divergence (DALI Z-score <17; Table S6), except *PbeAcXE* (root-mean-square deviation, RMSD 0.783 Å) and *CspAcXE* (RMSD 0.840 Å), which are well superposed with DacA_{pva} (Figure S7). However, the N-terminal loop1 of DacA_{pva} is considerably longer than those in *PbeAcXE* and *CspAcXE* (Figure S7). Targeted deletion of two amino acids at different positions within this loop resulted in a substantial loss of activity (Table S5), demonstrating the crucial role of loop1 in orienting the substrate within the active site. This finding is also consistent with the activity comparison analysis (Figure 1C), where DacA_{pva} exhibits higher activity toward PVA1788 than *PbeAcXE* and *CspAcXE*. It suggests that this N-terminal domain, with distinct loop 1, functions as a necessary domain for substrate binding and orientation.

Substrate-Binding Pocket of DacA_{pva}. To further understand the details of DacA_{pva} binding to polymers and its catalytic mechanism, we endeavored to obtain a crystal structure of DacA_{pva} in complex with polymer PVA1788. Although cocrystallization of WT-DacA_{pva} with PVA1788 failed, we successfully managed to cocrystallize the inactive mutant S227A with PVA1788. PVA1788 was trapped in the binding pocket of the enzyme, and two substrate fragments of different lengths were observed in the density maps shown in Figures S8 and S9. One of these two complexes contained a long chain of 22 carbons with two acetyl groups, which is designated C22-DacA_{pva-S227A} (Figure 2B). The other one contained a long chain of 15 carbons with one acetyl group and an acetate molecule, which is designated C15-ACT-DacA_{pva-S227A} (Figure 2C).

The overall structures of C22-DacA_{pva-S227A} and C15-ACT-DacA_{pva-S227A} closely resembled that of DacA_{pva} as indicated by the low RMSD values between each pair. Namely, the RMSD values for 375 Ca atoms and 368 Ca atoms were 0.087 and 0.131 Å, respectively. As to the comparison of these two complexes, superimposed structures between C22-DacA_{pva-S227A} and C15-ACT-DacA_{pva-S227A} exhibited little variations, particularly in the orientations of the hydroxyl and acetyl groups of PVA, as shown in Figure S10. These results

demonstrate that minimal conformational changes occurred among the different forms of DacA_{pva}. In particular, the conformation of loops around the substrate binding pocket is also relatively stable, of which an indistinctive migration of loop1 was seen in the structure of C15-ACT-DacA_{pva-S227A} (Figure S11). In the substrate-binding pocket, apart from the conserved catalytic triad (S227-D405-H408), residues D226, Y232, S266, G267, N303, V302, W310, Y355, Y356, S352, A351, and L407 were also observed around substrate PVA1788-C22 (Figure 2B). Based on interaction force analysis, each of N303 and H408 formed a hydrogen bond with the acetyl group, while S352 fixed the substrate by an additional hydrogen bond with another acetyl group. In addition, some hydrophobic residues were observed around the long-chain substrate PVA1788-C22, such as W310, Y355, Y356, Y232, and F307, suggesting that the hydrophobic interaction force played a primary role in the binding of the substrate. The residues around substrate PVA1788-C15 almost overlapped with the ones around PVA1788-C22, except for the absence of residue Y232 and the presence of extra F307 in the former (Figure 2B,C). Because these tightly coordinated residues assist in the binding of PVA1788, the polymer fragments PVA1788-C22 and PVA1788-C15 bound to this deacetylase can be observed in the crystal structure.

Structural Comparison of DacA_{pva} and Other Polymer Deacetylases. As the two enzymes most similar to DacA_{pva}, *CspAcXE* and *PbeAcXE*, are good targets for structural comparison. Electrostatic surface representations of C22-DacA_{pva-S227A}, MeGlcA-Xylp-*PbeAcXE*, and *CspAcXE* (notably, the active site structure of *CspAcXE* is incomplete) are shown in Figure 3 by APBS displayed in PyMOL (Version 3.0, Schrödinger, LLC). The surfaces surrounding the active site in

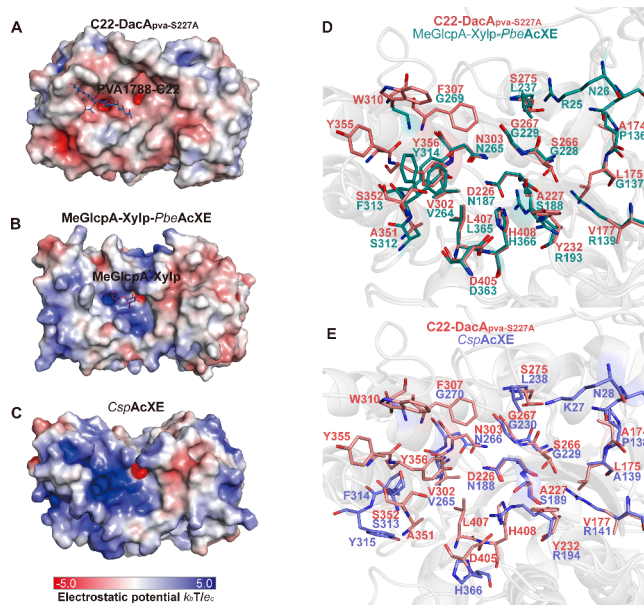


Figure 3. Structural comparison of DacA_{pva}, *PbeAcXE* and *CspAcXE*. Electrostatic potential surfaces of C22-DacA_{pva-S227A} (A, 9KR3), MeGlcA-Xylp-*PbeAcXE* (B, 7TOH), and *CspAcXE* (C, 7TOJ), where the surface charge distribution is displayed as blue for positive, red for negative, and white for neutral. Comparison of the binding pocket residues of C22-DacA_{pva-S227A} and MeGlcA-Xylp-*PbeAcXE* (D), C22-DacA_{pva-S227A} and *CspAcXE* (E). The bound residues are depicted as sticks: C22-DacA_{pva-S227A} (red), MeGlcA-Xylp-*PbeAcXE* (green), and *CspAcXE* (purple).

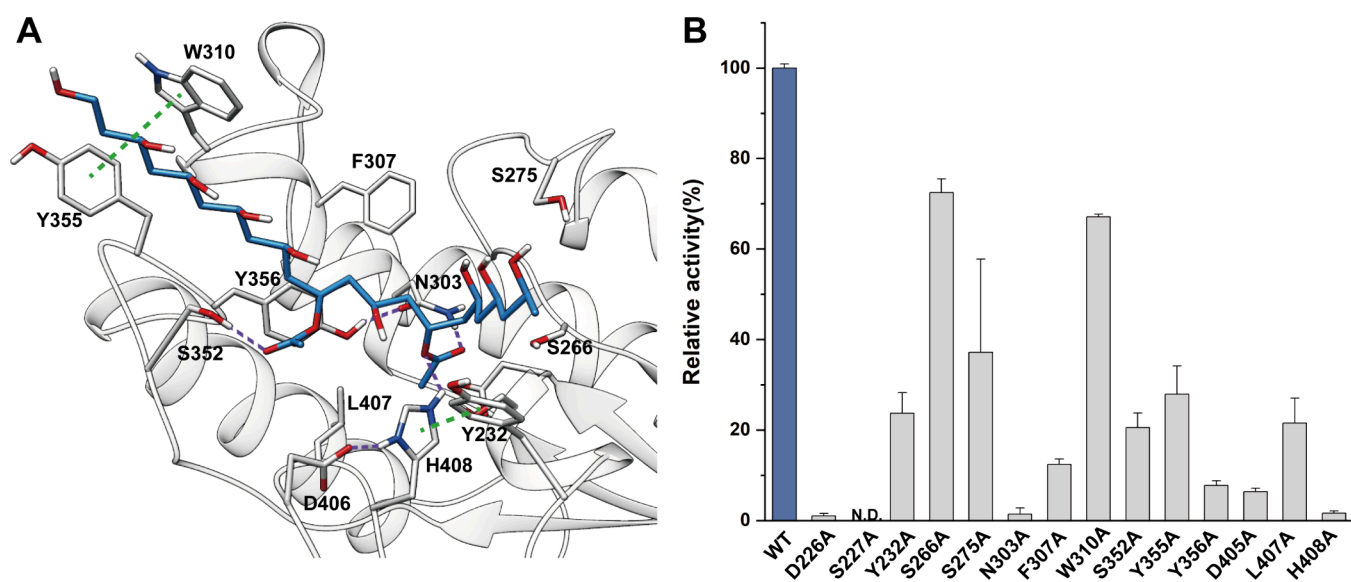


Figure 4. Analysis of mutation in key residues. (A) Residues in the active pocket of DacA_{pva} located within a 5 Å radius of the substrate were chosen for mutagenesis. (B) Activity of the mutants was determined. WT: wild-type DacA_{pva}. The activities are given as the standard deviation of three replicates.

PbeAcXE and *CspAcXE* are largely positively charged, while that in DacA_{pva} is largely negatively charged. Besides, the pocket of DacA_{pva} was more exposed, and the surrounding loops walled a circle of hydrophobic fences, which is favorable for binding the PVA substrate. This suggests that the strong, negatively charged pocket of DacA_{pva} binds the acetyl group, and the hydrophobic environment anchors the substrate backbone. Furthermore, a detailed sequence and structural comparison of these three enzymes shows a notable overlap between *PbeAcXE* and *CspAcXE*. However, substantial differences are observed between the binding pocket of DacA_{pva} and those of the other two enzymes (Figures S13 and S14). The substrate of MeGlcP-Xylp was bound into a positively charged environment, forming hydrogen bonds with R25, N26, R139, and R193 (Figure S14). The polymer PVA1788 relies on several CH- π interactions for anchoring, including at least four aromatic residues at loops 3, 5, and 6. Residue S352 formed a hydrogen bond with the acetyl side chain in the ligand-binding cavity of the DacA_{pva} (Figure S14). In the GH families, carbohydrate recognition based on arginine residues and aromatic residues is a distinguishing feature.³⁸ However, the conserved arginine residues in the pocket among members of this subfamily are absent in DacA_{pva}. Instead, three serine residues are present, likely to compensate for the lack of the arginine in specific loops: S266 and S275 at the loop 4, S352 at the loop 6. Serine can then be proposed as a substrate recognition residue in DacA_{pva} among the SGNH/GDSL superfamily.

In addition, other distantly related polysaccharide deacetylases, including CtCE2¹⁹ and RiCE17²¹ (Figure S15), as well as three cutinases (HiC, PmC, and FsC active toward PVA derivatives)³⁹ (Figure S16), were used to compare the active sites with DacA_{pva}. All these distant homologues were significantly different from DacA_{pva} in the overall structure. However, their binding pockets were all featured by the presence of hydrophobically aromatic residues, including tyrosine, tryptophan, and phenylalanine, implying their critical role in binding polymers.

Site-Directed Mutagenesis and Computational Analysis. To investigate the roles of key residues involved in substrate binding and catalysis, mutants of DacA_{pva} were tested for their activity toward the substrate PVA1788 (Figure 4). Whereas no detectable activity was observed for the mutant S227A, mutants N330A, D405A, and H408A retained no more than 10% of the WT activity. Additionally, Mutants Y232A, F307A, and Y356A retained about 30% activity, indicating that these aromatic residues contribute to the formation of an aromatic platform and are likely critical for stabilizing the substrate. On the other hand, W310 and Y355 are located at the entrance of the substrate pocket and form an aromatic clamp that may facilitate substrate binding. The W310A and Y355A mutants displayed a 30% reduction in activity, suggesting that the aromatic side chain of W310 and Y355 makes non-negligible contributions to stabilizing the substrate. As to the substrate-binding residues, S266, S275, and S352 were found to be important, with S352 playing a particularly crucial role. The S352A mutation led to a remarkable loss of activity, likely due to the disruption of a key hydrogen bond with the acetyl side chain of the substrate. This highlights the importance of these hydrogen bond interactions in substrate recognition and binding. The molecular mechanics-generalized born surface area (MM-GBSA) calculations were performed to assess the binding free energy of both DacA_{pva} and its mutants. Compared to WT, most of the mutants exhibit poorer binding free energy, which largely corroborates the experimental data, confirming that the residues implicated in activity loss contributed to the stability of the enzyme–substrate complex (Table S7).

Proposed Substrate Binding Mode and Enzymatic Mechanism. The hydrolysis mechanism of DacA_{pva} is mediated by the core Ser-His-Asp catalytic triad, where serine acts as the nucleophile, histidine functions as both the general base and acid, and aspartate assists in orienting the histidine residue while neutralizing the charge developed on histidine during the formation of transition states, in a way similar to previously described catalytic process.⁴⁰ This mechanism occurs in two major steps: the acylation and deacylation

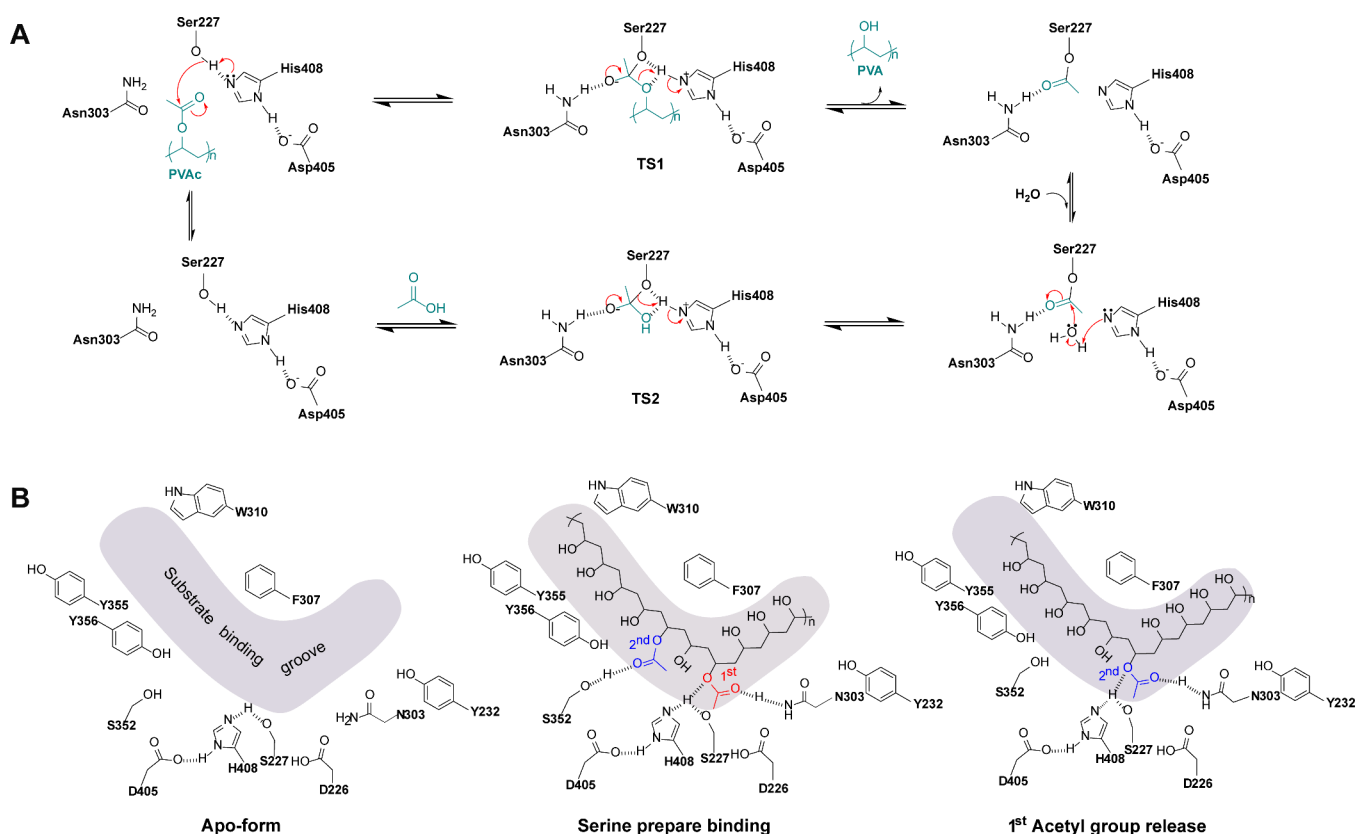


Figure 5. Catalytic mechanism of DacA_{pva}. (A) Proposed mechanism of DacA_{pva}-catalyzed deacetylation. (B) Model for deacetylation of polymer PVA by DacA_{pva}.

reactions. The formation of the tetrahedral transition state (TS1) and the breakdown of TS2 to release acetic acid both involve stabilization of the negatively charged oxygen by N303, akin to an oxyanion hole.⁴¹ The acyl-enzyme intermediate forms via TS1 and is released via TS2 (Figure 5A). Structural analysis of the WT protein cocrystallized with PVA1788 revealed additional electron density near the side chain of S227, consistent with the acyl-enzyme intermediate, where acetate is covalently attached to the hydroxyl oxygen of S227 (Figure 2D). The omit map of the acyl-enzyme intermediate and substrate- and product-bound states is shown in Figure 2D. These structural data provide crucial geometrical details that elucidate the catalytic mechanism.

Based on these findings, a catalytic pathway for DacA_{pva} is proposed (Figure 5B). An aromatic platform and serine interactions are initially formed in the apoenzyme, facilitating the binding of PVA1788 to the protein surface. Upon binding, the carbonyl group of the first acetyl side chain is directed toward the center of the substrate-binding pocket, where the catalytic triad mediates nucleophilic attack. The oxyanion hole polarizes the ester bond, stabilizing the reaction intermediate. The acyl-enzyme intermediate is then formed, followed by a second nucleophilic attack from a water molecule, consistent with the typical hydrolase mechanism. Simultaneously, the second acetyl side chain was anchored by S352, thereby priming the enzyme for the next catalytic cycle. Following cleavage of the first ester bond, the second acetyl side chain is drawn into stronger interactions with catalytic residues and the oxyanion hole, enabling its entry into the catalytic pocket and repetition of the catalytic process. This progressively slides the PVA1788 C–C backbone into the binding pocket, facilitating

the sequential removal of acetyl groups (Figure 5B). Compared to the arginine-carbohydrate interaction model used by *CspAcXE* and *PbeAcXE*, the serine prebinding model in this study may enhance the catalytic efficiency of DacA_{pva} on PVA1788 substrates.

Targeted molecular dynamics (TMD) simulations were widely applied to study the binding process between protein and ligand.⁴² To elucidate the molecular determinants for the unbinding kinetics of DacA_{pva}, we here combined experimental data with nonequilibrium TMD simulations on the enzyme with site-1 deacetylated-ligand PVA1788-C22. The nonequilibrium work obtained from TMD simulations converges quickly as expected. We monitored changes in the RMSD values (Figure S17A) to observe conformation fluctuations in the overall structure after TMD. The overall structure of the proteins is maintained in a stable state. The binding energy after TMD is $-28.13 \text{ kcal}\cdot\text{mol}^{-1}$, indicating the stability of the complex structure of TMD. The van der Waals interaction energy may exhibit key effects on binding kinetics: the presence of a long hydrophobic chain can either increase the residence time of the ligand by locking it to the protein or accelerate binding by facilitating the formation of a contracted form for fixing the ligand in the binding pocket. Meanwhile, the changes in the overall protein radius of gyration (Figure S17B) also indicate that the protein–ligand complex conformation has reached an equilibrium state.

CONCLUSIONS

The structural elucidation of DacA_{pva} and its complex with PVA has provided a model for understanding how a plastic-modifying enzyme binds to its polymer substrate. DacA_{pva}

exhibits a dual-domain architecture comprising an SGNH superfamily hydrolytic domain and a unique N-terminal domain, ensuring the structural integrity of the protein. The superior ability of DacA_{pva} to bind C–C backbone substrates can be attributed to the presence of an aromatic platform surrounding the substrate binding pocket and the catalytic force exerted by serine residues. A novel mechanism for DacA_{pva} catalysis was elucidated through crystal structure analysis and stretching kinetics simulations. This mechanism involves serine prebinding and the sequential removal of acetyl groups by polymer sliding within the enzyme pocket. Understanding of this unique mechanism advances our knowledge of rarely observed polymer-enzyme interactions and provides a valuable template for engineering enzymes for plastic modification.

■ ASSOCIATED CONTENT

SI Supporting Information

The Supporting Information is available free of charge at <https://pubs.acs.org/doi/10.1021/acscatal.5c01764>.

Details on the general processes of poly(vinyl alcohol) synthesis, biodegradation, and upcycling; figures illustrating SDS-PAGE of DacA_{pva} mutants, structural characterization, enzymatic assays, molecular docking, sequence and structure alignments, electron density maps, binding pocket analyses, and molecular dynamic simulations; and tables of details for substrates and primers used in this study, crystallization data, activity assays, structural homologues, and binding free energy results (PDF)

■ AUTHOR INFORMATION

Corresponding Authors

Ning-Yi Zhou – State Key Laboratory of Microbial Metabolism, Joint International Research Laboratory of Metabolic and Developmental Sciences, and School of Life Sciences and Biotechnology, Shanghai Jiao Tong University, Shanghai 200240, China; orcid.org/0000-0002-0917-5750; Email: ningyi.zhou@sjtu.edu.cn

Jiahai Zhou – State Key Laboratory of Microbial Technology, Nanjing Normal University, Nanjing 210023, China; Shenzhen Institute of Synthetic Biology, Shenzhen Institutes of Advanced Technology, Chinese Academy of Sciences, Shenzhen 518055, China; Email: jiahai@nnu.edu.cn

Authors

Yanfei Wu – State Key Laboratory of Microbial Metabolism, Joint International Research Laboratory of Metabolic and Developmental Sciences, and School of Life Sciences and Biotechnology, Shanghai Jiao Tong University, Shanghai 200240, China; Shenzhen Institute of Synthetic Biology, Shenzhen Institutes of Advanced Technology, Chinese Academy of Sciences, Shenzhen 518055, China

Xuexia Xu – State Key Laboratory of Microbial Technology, Nanjing Normal University, Nanjing 210023, China

Chao-Fan Yin – State Key Laboratory of Microbial Metabolism, Joint International Research Laboratory of Metabolic and Developmental Sciences, and School of Life Sciences and Biotechnology, Shanghai Jiao Tong University, Shanghai 200240, China

Zhuanglin Shen – Shenzhen Institute of Synthetic Biology, Shenzhen Institutes of Advanced Technology, Chinese Academy of Sciences, Shenzhen 518055, China

Lanteng Wang – Shenzhen Institute of Synthetic Biology, Shenzhen Institutes of Advanced Technology, Chinese Academy of Sciences, Shenzhen 518055, China;

orcid.org/0000-0001-6603-7787

Complete contact information is available at: <https://pubs.acs.org/10.1021/acscatal.5c01764>

Author Contributions

[¶]Y.W., X.X., and C.-F.Y. contributed equally to this work. Y.W. performed protein purification, crystallization, diffraction data collection and analysis, and contributed to manuscript writing. X.X. performed molecular docking, binding free energy calculation and TMD simulations, and contributed to manuscript writing. C.-F.Y. performed enzyme activity assays and contributed to manuscript writing. L.W. assisted with structure determination. Z.S. assisted with computer analysis. J.Z. and N.Z. supervised the project, designed the study, and wrote the manuscript.

Notes

The authors declare no competing financial interest.

■ ACKNOWLEDGMENTS

This work was supported by grants from the National Key R&D Program of China (2024YFA0919000 to N.Z.), Jiangsu Basic Research Center for Synthetic Biology (BK20233003 to J.Z.), and the Seed Industry Revitalization Project of Guangdong Province (23050202 to N.Z.). We thank the staff members of beamline BL19U1 of Shanghai Synchrotron Radiation Facility for their assistance and help during X-ray data collection.

■ REFERENCES

- (1) Borrelle, S. B.; Ringma, J.; Law, K. L.; Monnahan, C. C.; Lebreton, L.; McGivern, A.; Murphy, E.; Jambeck, J.; Leonard, G. H.; Hilleary, M. A.; Eriksen, M.; Possingham, H. P.; De Frond, H.; Gerber, L. R.; Polidoro, B.; Tahir, A.; Bernard, M.; Mallos, N.; Barnes, M.; Rochman, C. M. Predicted growth in plastic waste exceeds efforts to mitigate plastic pollution. *Science* **2020**, 369 (6510), 1515–1518.
- (2) Jehanno, C.; Alty, J. W.; Roosen, M.; De Meester, S.; Dove, A. P.; Chen, E. Y. X.; Leibfarth, F. A.; Sardon, H. Critical advances and future opportunities in upcycling commodity polymers. *Nature* **2022**, 603 (7903), 803–814.
- (3) Ellis, L. D.; Rorrer, N. A.; Sullivan, K. P.; Otto, M.; McGeehan, J. E.; Román-Leshkov, Y.; Wierckx, N.; Beckham, G. T. Chemical and biological catalysis for plastics recycling and upcycling. *Nat. Catal.* **2021**, 4 (7), 539–556.
- (4) Liu, J. W.; He, J.; Xue, R.; Xu, B.; Qian, X. J.; Xin, F. X.; Blank, L. M.; Zhou, J.; Wei, R.; Dong, W. L.; Jiang, M. Biodegradation and upcycling of polyurethanes: Progress, challenges, and prospects. *Biotechnol. Adv.* **2021**, 48, No. 107730.
- (5) Tiso, T.; Narancic, T.; Wei, R.; Pollet, E.; Beagan, N.; Schröder, K.; Honak, A.; Jiang, M. Y.; Kenny, S. T.; Wierckx, N.; Perrin, R.; Avérous, L.; Zimmermann, W.; O'Connor, K.; Blank, L. M. Towards bio-upcycling of polyethylene terephthalate. *Metab. Eng.* **2021**, 66, 167–178.
- (6) Rosenboom, J. G.; Langer, R.; Traverso, G. Bioplastics for a circular economy. *Nat. Rev. Mater.* **2022**, 7 (2), 117–137.
- (7) Teodorescu, M.; Bercea, M.; Morariu, S. Biomaterials of Poly(vinyl alcohol) and Natural Polymers. *Polym. Rev.* **2018**, 58 (2), 247–287.

- (8) Rostagno, M.; Shen, S.; Ghiviriga, I.; Miller, S. A. Sustainable poly(vinyl) acetals from bioaromatic aldehydes. *Polym. Chem.* **2017**, *8* (34), 5049–5059.
- (9) Amann, M.; Minge, O. Biodegradability of Poly(vinyl acetate) and Related Polymers. *Synthetic Biodegradable Polymers* **2011**, *245*, 137–172.
- (10) Cheng, H. N. Enzymatic Modification of Polymers. In *Enzymatic Polymerization towards Green Polymer Chemistry*; Kobayashi, S.; Uyama, H.; Kadokawa, J.-i., Eds.; Singapore: Springer Singapore, 2019; pp 357–385.
- (11) Chen, C.-C.; Dai, L.; Ma, L.; Guo, R.-T. Enzymatic degradation of plant biomass and synthetic polymers. *Nat. Rev. Chem.* **2020**, *4* (3), 114–126.
- (12) Tournier, V.; Duquesne, S.; Guillaumot, F.; Cramail, H.; Taton, D.; Marty, A.; André, I. Enzymes' Power for Plastics Degradation. *Chem. Rev.* **2023**, *123* (9), 5612–5701.
- (13) Austin, H. P.; Allen, M. D.; Donohoe, B. S.; Rorrer, N. A.; Kearns, F. L.; Silveira, R. L.; Pollard, B. C.; Dominick, G.; Duman, R.; El Omari, K.; Mykhaylyk, V.; Wagner, A.; Michener, W. E.; Amore, A.; Skaf, M. S.; Crowley, M. F.; Thorne, A. W.; Johnson, C. W.; Woodcock, H. L.; McGeehan, J. E.; Beckham, G. T. Characterization and engineering of a plastic-degrading aromatic polyesterase. *Proc. Natl. Acad. Sci. U.S.A.* **2018**, *115* (19), E4350–E4357.
- (14) Ben Halima, N. Poly(vinyl alcohol): review of its promising applications and insights into biodegradation. *RSC Adv.* **2016**, *6* (46), 39823–39832.
- (15) von Haugwitz, G.; Donnelly, K.; Di Filippo, M.; Breite, D.; Phippard, M.; Schulze, A.; Wei, R.; Baumann, M.; Bornscheuer, U. T. Synthesis of Modified Poly(vinyl Alcohol)s and Their Degradation Using an Enzymatic Cascade. *Angew. Chem., Int. Ed.* **2023**, *62* (18), No. e202216962.
- (16) Yin, C.-F.; Xu, Y.; Deng, S.-K.; Yue, W.-L.; Zhou, N.-Y. A novel esterase DacA_{pva} from *Comamonas* sp. strain NyZ500 with deacetylation activity for acetylated polymer polyvinyl alcohol. *Appl. Environ. Microbiol.* **2021**, *87* (8), No. e03016-20.
- (17) Akoh, C. C.; Lee, G. C.; Liaw, Y. C.; Huang, T. H.; Shaw, J. F. GDSL family of serine esterases/lipases. *Prog. Lipid Res.* **2004**, *43* (6), 534–552.
- (18) Anderson, A. C.; Stangherlin, S.; Pimentel, K. N.; Weadge, J. T.; Clarke, A. J. The SGNH hydrolase family: a template for carbohydrate diversity. *Glycobiology* **2022**, *32* (10), 826–848.
- (19) Montanier, C.; Money, V. A.; Pires, V. M. R.; Flint, J. E.; Pinheiro, B. A.; Goyal, A.; Prates, J. A. M.; Izumi, A.; Stålbbrand, H.; Morland, C.; Cartmell, A.; Kolenova, K.; Topakas, E.; Dodson, E. J.; Bolam, D. N.; Davies, G. J.; Fontes, C. M. G. A.; Gilbert, H. J. The Active Site of a Carbohydrate Esterase Displays Divergent Catalytic and Noncatalytic Binding Functions. *PLoS Biol.* **2009**, *7* (3), No. e1000071.
- (20) Penttinen, L.; Kouhi, V.; Fauré, R.; Skarina, T.; Stogios, P.; Master, E.; Jurak, E. Elucidating Sequence and Structural Determinants of Carbohydrate Esterases for Complete Deacetylation of Substituted Xylans. *Molecules* **2022**, *27* (9), 2655.
- (21) Michalak, L.; La Rosa, S. L.; Leivers, S.; Lindstad, L. J.; Røhr, Å. K.; Lillelund Aachmann, F.; Westereng, B. A pair of esterases from a commensal gut bacterium remove acetylations from all positions on complex β -mannans. *Proc. Natl. Acad. Sci. U. S. A.* **2020**, *117* (13), 7122–7130.
- (22) Minor, W.; Cymborowski, M.; Otwinowski, Z.; Chruszcz, M. HKL-3000: the integration of data reduction and structure solution–from diffraction images to an initial model in minutes. *Acta Crystallogr., Sect. D: Biol. Crystallogr.* **2006**, *62* (Pt 8), 859–866.
- (23) Kabsch, W. XDS. *Acta Crystallogr., Sect. D: Biol. Crystallogr.* **2010**, *66* (Pt 2), 125–132.
- (24) McCoy, A. J.; Grosse-Kunstleve, R. W.; Adams, P. D.; Winn, M. D.; Storoni, L. C.; Read, R. J. Phaser crystallographic software. *J. Appl. Crystallogr.* **2007**, *40* (Pt 4), 658–674.
- (25) Emsley, P.; Lohkamp, B.; Scott, W. G.; Cowtan, K. Features and development of Coot. *Acta Crystallogr., Sect. D: Biol. Crystallogr.* **2010**, *66* (Pt 4), 486–501.
- (26) Afonine, P. V.; Grosse-Kunstleve, R. W.; Echols, N.; Headd, J. J.; Moriarty, N. W.; Mustyakimov, M.; Terwilliger, T. C.; Urzhumtsev, A.; Zwart, P. H.; Adams, P. D. Towards automated crystallographic structure refinement with phenix.refine. *Acta Crystallogr., Sect. D: Biol. Crystallogr.* **2012**, *68* (Pt 4), 352–367.
- (27) Afonine, P. V.; Grosse-Kunstleve, R. W.; Chen, V. B.; Headd, J. J.; Moriarty, N. W.; Richardson, J. S.; Richardson, D. C.; Urzhumtsev, A.; Zwart, P. H.; Adams, P. D. phenix.model_vs_data: a high-level tool for the calculation of crystallographic model and data statistics. *J. Appl. Crystallogr.* **2010**, *43* (Pt 4), 669–676.
- (28) Jumper, J.; Evans, R.; Pritzel, A.; Green, T.; Figurnov, M.; Ronneberger, O.; Tunyasuvunakool, K.; Bates, R.; Zidek, A.; Potapenko, A.; Bridgland, A.; Meyer, C.; Kohl, S. A. A.; Ballard, A. J.; Cowie, A.; Romera-Paredes, B.; Nikolov, S.; Jain, R.; Adler, J.; Back, T.; Petersen, S.; Reiman, D.; Clancy, E.; Zielinski, M.; Steinegger, M.; Pacholska, M.; Berghammer, T.; Bodenstein, S.; Silver, D.; Vinyals, O.; Senior, A. W.; Kavukcuoglu, K.; Kohli, P.; Hassabis, D. Highly accurate protein structure prediction with AlphaFold. *Nature* **2021**, *596* (7873), 583–589.
- (29) Trott, O.; Olson, A. J. Software News and Update AutoDock Vina: Improving the Speed and Accuracy of Docking with a New Scoring Function, Efficient Optimization, and Multithreading. *J. Comput. Chem.* **2010**, *31* (2), 455–461.
- (30) Eberhardt, J.; Santos-Martins, D.; Tillack, A. F.; Forli, S. AutoDock Vina 1.2.0: New Docking Methods, Expanded Force Field, and Python Bindings. *J. Chem. Inf. Model.* **2021**, *61* (8), 3891–3898.
- (31) Yang, M. H.; Bo, Z. H.; Xu, T.; Xu, B.; Wang, D. D.; Zheng, H. Uni-GBSA: an open-source and web-based automatic workflow to perform MM/GB(PB)SA calculations for virtual screening. *Briefings Bioinf.* **2023**, *24* (4), No. bbad218.
- (32) Wolf, S.; Amaral, M.; Lowinski, M.; Vallee, F.; Musil, D.; Guldenhaupt, J.; Dreyer, M. K.; Bomke, J.; Frech, M.; Schlitter, J.; Gerwert, K. Estimation of Protein-Ligand Unbinding Kinetics Using Non-Equilibrium Targeted Molecular Dynamics Simulations. *J. Chem. Inf. Model.* **2019**, *59* (12), 5135–5147.
- (33) Phillips, J. C.; Braun, R.; Wang, W.; Gumbart, J.; Tajkhorshid, E.; Villa, E.; Chipot, C.; Skeel, R. D.; Kale, L.; Schulten, K. Scalable molecular dynamics with NAMD. *J. Comput. Chem.* **2005**, *26* (16), 1781–1802.
- (34) Darden, T.; York, D.; Pedersen, L. Particle Mesh Ewald - an $N \log(N)$ Method for Ewald Sums in Large Systems. *J. Chem. Phys.* **1993**, *98* (12), 10089–10092.
- (35) Hou, T.; Wang, J.; Li, Y.; Wang, W. Assessing the performance of the MM/PBSA and MM/GBSA methods. 1. The accuracy of binding free energy calculations based on molecular dynamics simulations. *J. Chem. Inf. Model.* **2011**, *51* (1), 69–82.
- (36) Salomon-Ferrer, R.; Case, D. A.; Walker, R. C. An overview of the Amber biomolecular simulation package. *WIREs Comput. Mol. Sci.* **2013**, *3* (2), 198–210.
- (37) Ernst, H. A.; Mosbech, C.; Langkilde, A. E.; Westh, P.; Meyer, A. S.; Agger, J. W.; Larsen, S. The structural basis of fungal glucuronoyl esterase activity on natural substrates. *Nat. Commun.* **2020**, *11* (1), 1026.
- (38) Vieira, P. S.; Bonfim, I. M.; Araujo, E. A.; Melo, R. R.; Lima, A. R.; Fessel, M. R.; Paixao, D. A. A.; Persinoti, G. F.; Rocco, S. A.; Lima, T. B.; Pirolla, R. A. S.; Morais, M. A. B.; Correa, J. B. L.; Zanthorlin, L. M.; Diogo, J. A.; Lima, E. A.; Grandis, A.; Buckeridge, M. S.; Gozzo, F. C.; Benedetti, C. E.; Polikarpov, I.; Giuseppe, P. O.; Murakami, M. T. Xyloglucan processing machinery in pathogens and its role in the transcriptional activation of virulence factors. *Nat. Commun.* **2021**, *12* (1), 4049.
- (39) Ronkvist, Å. M.; Lu, W.; Feder, D.; Gross, R. A. Cutinase-Catalyzed Deacetylation of Poly(vinyl acetate). *Macromolecules* **2009**, *42* (16), 6086–6097.
- (40) Rauwerdink, A.; Kazlauskas, R. J. How the Same Core Catalytic Machinery Catalyzes 17 Different Reactions: the Serine-Histidine-Aspartate Catalytic Triad of α/β -Hydrolase Fold Enzymes. *ACS Catal.* **2015**, *5* (10), 6153–6176.

(41) Zong, Z.; Mazurkewich, S.; Pereira, C. S.; Fu, H.; Cai, W.; Shao, X.; Skaf, M. S.; Larsbrink, J.; Lo Leggio, L. Mechanism and biomass association of glucuronoyl esterase: an α/β hydrolase with potential in biomass conversion. *Nat. Commun.* **2022**, *13* (1), 1449.

(42) Gohlke, H.; Klebe, G. Approaches to the description and prediction of the binding affinity of small-molecule ligands to macromolecular receptors. *Angew. Chem., Int. Ed.* **2002**, *41* (15), 2644–2676.